

AD-A162 452 COMPARISON OF A VERY HIGH FREQUENCY 148 MHZ INDUCTIVELY COUPLED PLASMA(U) ARIZONA UNIV TUCSON DEPT OF CHEMISTRY 1/1  
B D WEBB ET AL 26 NOV 85 TR-43 N00014-83-K-0268

AD-A162 452 COMPARISON OF A VERY HIGH FREQUENCY 148 MHZ INDUCTIVELY COUPLED PLASMA(U) ARIZONA UNIV TUCSON DEPT OF CHEMISTRY 1/1  
B D WEBB ET AL 26 NOV 85 TR-43 N00014-83-K-0268

AD-A162 452 COMPARISON OF A VERY HIGH FREQUENCY 148 MHZ INDUCTIVELY COUPLED PLASMA(U) ARIZONA UNIV TUCSON DEPT OF CHEMISTRY 1/1  
B D WEBB ET AL 26 NOV 85 TR-43 N00014-83-K-0268

UNCLASSIFIED F/G 20/9 NL

UNCLASSIFIED F/G 20/9 NL

UNCLASSIFIED F/G 20/9 NL

[illegible]



REPORT D

READ INSTRUCTIONS  
BEFORE COMPLETING FORM

RECIPIENT'S CATALOG NUMBER

1. REPORT NUMBER

43

AD-A162 452

4. TITLE (and Subtitle)

Comparison of a Very High Frequency 148 MHz  
Inductively Coupled Plasma

5. TYPE OF REPORT &amp; PERIOD COVERED

Interim

6. PERFORMING ORG. REPORT NUMBER

7. AUTHOR(s)

B.D. Webb and M.B. Denton

8. CONTRACT OR GRANT NUMBER(s)

N00014-83-K-0262

9. PERFORMING ORGANIZATION NAME AND ADDRESS

Department of Chemistry  
University of Arizona  
Tucson, Arizona 8572110. PROGRAM ELEMENT, PROJECT, TASK  
AREA & WORK UNIT NUMBERS

NR 051-549

11. CONTROLLING OFFICE NAME AND ADDRESS

Office of Naval Research  
Arlington, Virginia 22217

12. REPORT DATE

November 26, 1985

13. NUMBER OF PAGES

49

14. MONITORING AGENCY NAME &amp; ADDRESS (if different from Controlling Office)

15. SECURITY CLASS. (of this report)

Unclassified

15a. DECLASSIFICATION/DOWNGRADING  
SCHEDULE

16. DISTRIBUTION STATEMENT (of this Report)

This document has been approved for public release and sale;  
its distribution is unlimited.

17. DISTRIBUTION STATEMENT (of the abstract entered in Block 20, if different from Report)

18. SUPPLEMENTARY NOTES

Accepted for publication in Spectrochimica Acta - Part B

19. KEY WORDS (Continue on reverse side if necessary and identify by block number)

Inductively Coupled Plasma (ICP)

20. ABSTRACT (Continue on reverse side if necessary and identify by block number)

Physical parameters and analytical performance are determined for an analytical ICP operated at 148 MHz, a frequency nearly three times higher than any previously reported. The iron(I) excitation temperatures are approximately 1.5 times lower and the electron densities are five times lower than at 27 MHz. The consequences of these changes are lower analyte and background continuum emission intensities, such that the signal to background ratios are decreased at the higher frequency. Freedom from interferences and working curve linearity are unaffected while ease of sample introduction is improved. A shift towards atomic emission

(See other side)

DD FORM 1 JAN 73 1473

EDITION OF 1 NOV 68 IS OBSOLETE

S/N 0102- LF-014-6601

SECURITY CLASSIFICATION OF THIS PAGE (When Data Entered)

TOP FILE COPY

DTIC  
ELECTE  
S DEC 18 1985 D

Indicates a deviation farther from LTE at 148 MHz. These effects are attributed to the decrease in skin depth with increasing frequency.

OFFICE OF NAVAL RESEARCH

Contract N00014-83-K-0268

Task No. 051-549

TECHNICAL REPORT NO. 43

Comparison of a Very High Frequency 148 MHz  
Inductively Coupled Plasma to a 27 MHz ICP

by

B. D. Webb and M. B. Denton

Accepted for publication in  
Spectrochimica Acta - Part B

Department of Chemistry  
University of Arizona  
Tucson, Arizona 85721

DTIC  
ELECTE  
S DEC 18 1985 D

November 26, 1985

Reproduction in whole or in part is permitted for  
any purpose of the United States Government.

\*This document has been approved for public release  
and sale; its distribution is unlimited.

85 12 17 123

## ABSTRACT

Physical parameters and analytical performance are determined for an analytical ICP operated at 148 MHz, a frequency nearly three times higher than any previously reported. The iron(I) excitation temperatures are approximately 1.5 times lower and the electron densities are 5 times lower than at 27 MHz. The consequences of these changes are lower analyte and background continuum emission intensities, such that the signal to background ratios are decreased at the higher frequency. Freedom from interferences and working curve linearity are unaffected while ease of sample introduction is improved. A shift towards atomic emission indicates a deviation farther from LTE at 148 MHz. These effects are attributed to the decrease in skin depth with increasing frequency.

Accession For	
NTIS	CRA&I <input checked="" type="checkbox"/>
DTIC	TAB <input type="checkbox"/>
Unannounced <input type="checkbox"/>	
Justification	
By	
Distribution /	
Availability Codes	
Dist	Avail and/or Special
A-1	

## 1. INTRODUCTION

Much progress has been made in the field of ICP-AES in the two decades since REED's first reports [1,2]. Plasmas have been operated at a wide range of frequencies since his work at 4 MHz, with most systems today operating at a frequency of 27 MHz. The recent trend towards higher frequency operation of ICPs is due to a change in the energy deposition region with frequency. It is useful to think of the energy deposition region in terms of the skin depth, which is defined as the distance required for the induced field strength to fall off to  $1/e$  of its value at the surface, and is inversely proportional to the square root of the discharge frequency [3]. All other factors being equal, increasing the generator frequency moves the primary energy deposition region farther towards the outside of the plasma. One of the advantages of a reduced skin depth is that the analyte, which is injected along the central channel, is less likely to perturb the energy deposition process, and sample introduction is therefore easier at higher frequencies. The tradeoff is that the analyte consequently experiences a lower energy environment. CAPELLE *et al.* [4] have investigated the influence of generator frequency at 5, 27, 40, 50 and 56 MHz and found that analytical performance is improved at 56 MHz compared to 27 MHz. GUNTER *et al.* [5] compared 9, 27 and 50 MHz ICPs and observed similar trends in excitation temperature and electron number density. This manuscript characterizes the operation of an ICP at 148 MHz, nearly three

times the highest frequency investigated in previous studies, affording an extended view of the effect of generator frequency on the plasma.

The physical parameters of excitation temperature, electron number density, and ion-to-atom line intensity ratios have been determined at several power levels for the two frequencies of 27 MHz and 148 MHz. A number of potential variables are held constant by using the same optical system and thermometric species at each frequency, allowing a meaningful comparison of the two ICPs. In order to determine the consequences of the changes in the physical parameters, analytical performance has been evaluated for several elements in terms of signal-to-background ratios, detection limits, calibration curves, and effect of interferences. Ease of organic sample introduction is also evaluated.

## 2. APPARATUS and TECHNIQUES

(All of section 2 may be printed in smaller type)

### 2.1. Instrumentation

The 27 MHz RF generator, matching network, and standard size torch were identical to the ones previously described [6,7]. While the 27 MHz generator allows a continuous adjustment of power level, the 148.26 MHz crystal-controlled RF generator, a Hughes (Fullerton, CA) model HC-300B VHF Command Transmitter, provides a more limited choice of six switch-selected output power levels of 250, 400, 550, 900, 1200, 1500, and 2000 watts. The matching network was modified to operate at 148 MHz by replacing the 2-1/2



turn load coil with a one-turn coil, and the output pi-network vacuum variable capacitor was replaced with a variable air-gap capacitor machined from 6 mm thick copper plates 80 mm in diameter, spaced by approximately 16 mm.

The same torch was used in both systems, and was mounted in a shielded enclosure on two Velmex, Inc. (East Bloomfield, NY) dovetail slides driven by Rapid-Syn (Oceanside, CA) stepper motors controlled by a Denco Research, Inc. (Tucson, AZ) SM-2A controller. This allows computer-controlled positioning of the torch vertically and laterally with respect to the optical axis. A 75 mm diameter x 120 mm focal length quartz lens was used to image the plasma with 1:1 magnification onto the entrance slit of a GCA-McPherson (Acton, MA) EU-700 monochromator equipped with a Hamamatsu (Middlesex, NJ) R212 photomultiplier tube. The electrometer, analog-to-digital converter, and computer system are similar to those described by HEINE et al. [7]. All data were taken under computer control utilizing routines written in CONVERS [8].

The nebulizer is of cross-flow design constructed in our laboratory, with a sample uptake rate of 1.3 mL/min and an aerosol output of 1.1 L/min. A variable vent is placed on the spray chamber to regulate the actual flow to the plasma. A nebulizer gas flow of 0.7 L/min was used for both frequencies. Coolant gas flow was approximately 12 L/min and no auxiliary gas was needed.

## 2.2. Excitation Temperatures

Iron was chosen as the primary thermometric species for three reasons: (1) many spectral lines are available in a small wavelength region, so correction for the variation of instrumental response with wavelength is not necessary, (2) the transition probabilities for iron are generally more reliable, and (3) many previous studies of the ICP have used iron so direct comparison of results is possible. Excitation temperatures were determined by the slope method [9,10] with a linear-least-squares fit, in which  $\ln(g_u A_{ul}/I\lambda)$  is plotted versus excitation energy of the spectral lines, and the slope is equal to  $1/kT$ . For a transition from upper level  $u$  to lower level  $l$ ,  $I$  is spectral line intensity,  $\lambda$  is the wavelength,  $g_u$  and  $g_l$  are the statistical weights of each level, and  $A_{ul}$  is the transition probability for spontaneous emission. Transition probability data are often reported as  $\log_{10}(g_l f_{lu})$ , where  $f_{lu}$  is the oscillator strength and is related to the transition probability by:

$$g_l f_{lu} = 1.499 \times 10^{-14} \lambda^2 g_u A_{ul} \quad (1)$$

when  $A_{ul}$  is in  $\text{sec}^{-1}$  and  $\lambda$  is in nm. Hence  $\ln(g_l f_{lu}/I\lambda^3)$  can be plotted instead of  $\ln(g_u A_{ul}/I\lambda)$  if  $\log(g_l f_{lu})$  values are available.  $I$ ,  $\lambda$ , and  $g_l f_{lu}$  may be on relative scales, but if  $E_{\text{exc}}$  is expressed in  $\text{cm}^{-1}$  and  $T$  in Kelvin, the slope will be  $1.4394/T$ . The relative standard deviation of the slope of the line can be used to calculate an estimated error,  $\Delta T$ . The spectroscopic constants of the lines used are shown in Table 1.

Many of the earlier studies of excitation temperature in the ICP have utilized the transition probability data of CORLISS and BOZMAN [11] or CORLISS and TECH [12], but a systematic error in this compilation generally leads to lower values of excitation temperature than the corrected data [13]. More recent transition probabilities from BRIDGES and KORNBLITH [14] have been judged to be more accurate and the data from BLACKWELL *et al.* [15-21] to be most accurate in a critical compilation of iron transition probability data [22]. Another commonly used set of transition probabilities is from REIF *et al.* [23]. The least uncertainty  $\Delta T$  is obtained using the critically evaluated transition probabilities [22] with the data obtained in the present study. Slightly higher excitation temperatures but larger uncertainties are obtained using transition probability values from REIF *et al.* or BRIDGES and KORNBLITH, while larger uncertainties and markedly lower temperatures are obtained using the older values [11]. This is in agreement with another recent study of temperatures in the ICP using a Fourier transform spectrometer by FAIRES *et al.* [24].

Lateral profiles of the six wavelengths taken at several observation heights were Abel inverted [25] and the inverted intensities used to calculate new excitation temperatures. The inverted temperatures were within the same error bars in each case, so Abel inversion was deemed unnecessary for injected elements viewed on axis, in agreement with an earlier study [10].

Figure 1 shows a comparison of the results obtained from a representative data set of the Fe(I) lines analyzed with the various different sets of transition probabilities. The error bars on the plot

correspond to the uncertainties in the temperatures calculated at each observation height. These results are very comparable in magnitude to those presented in the study by FAIRES *et al.* [24] when using the same transition probabilities.

As a check on the iron excitation temperatures, six lines of titanium ion emission were also used. Spectroscopic data for these lines are shown in Table 2. Transition probabilities are less accurately known for titanium, so there is more uncertainty in these results. A critical compilation [26] indicated better transition probabilities from the work of ROBERTS *et al.* [27,28] but a much better fit is obtained with the data of WARNER [29]. This again is in agreement with an earlier study [10].

A similar excitation temperature is obtained with the titanium ion as with the iron atom emission, as can be seen in Fig. 2 for two different power levels. The higher titanium temperatures at the lower observation heights may be due to the much lower emission there coupled with the much higher sloping spectral background, giving anomalous peak heights in the data collection routine.

### 2.3. Electron Densities

Electron densities can be determined on an absolute scale by measuring the Stark broadening of a suitable spectral line [30-32]. Hydrogen  $H\beta$  at 486.13 nm is sufficiently broadened in the ICP to allow measurement of the line profile with a medium resolution spectrometer. Water was aspirated into the plasma for these measurements, but hydrogen was not added to the plasma as is often done because it radically altered the shape of the

discharge even at low concentrations, and did not enhance the H emission. A slit width of 25 microns was used at 27 MHz, while 35 microns was used at 148 MHz to compensate for the weaker emission at the higher frequency, giving instrumental half-widths of 0.05 and 0.07 nm, respectively. The Doppler broadening contribution can be calculated from the relationship:

$$\Delta\lambda_{1/2}^D = 7.17 \times 10^{-7} \lambda (T/m)^{1/2} \quad (2)$$

where  $T$  is in K and  $m$  in atomic units [30]. This is not very sensitive to temperature, and a half-width of 0.025 nm calculated from a temperature of 5000 K was assumed for all measurements. These half-widths when deconvolved from the experimentally observed half-width then give the Stark half-width,  $\Delta\lambda_{1/2}^S$ , which is related to the electron density,  $n_e$ , by:

$$\Delta\lambda_{1/2}^S = 2.50 \times 10^{-10} \alpha_{1/2} n_e^{2/3} \quad (3)$$

where  $\Delta\lambda_{1/2}^S$  is in nm and  $n_e$  is in  $\text{cm}^{-3}$  [30]. The half-width parameter  $\alpha_{1/2}$  can be obtained from tabulations of the theoretical line profile [31-33]. Since  $\alpha_{1/2}$  is somewhat dependent on temperature and electron density, an iterative technique has most often been employed [10,34,35]. With the data from the present study, the error caused by an order of magnitude change in assumed electron density or temperature was only 4 percent compared to 10 percent from the uncertainty in determining the half-widths, so the use of a single relationship as plotted by WIESE [30] is justified. The relationship between observed half-width and electron density is quantified as:

$$\log_{10}(n_e) = 1.431 \log_{10}(\Delta\lambda_{1/2}^S) + 16.000 \quad (4)$$

when  $\Delta\lambda_{1/2}^S$  is expressed in nm. The overall uncertainty in  $n_e$  is estimated to be less than 20 percent. Based on the results of the excitation temperature study, Abel inversions were not deemed necessary.

#### 2.4. Signal to Background Ratios

Signal to background ratios were determined for several elements under compromise conditions of 1000 W at 27 MHz and 1200 W at 148 MHz. Two analog-to-digital converters were used to obtain the S/B ratios because of the wide dynamic range involved. One ADC digitized the total analyte-plus-background signal above a zero set with the light beam blocked. The other, set to ten times the sensitivity of the first, digitized the background signal at a nearby wavelength previously determined to have the same intensity as at the analyte line. This procedure was then repeated for the range of observation heights.

#### 2.5. Theoretical LTE Temperatures

The Saha-Eggert relationship may be used to describe the equilibrium between the successive ionization stages of an analyte or the argon support gas. Assuming Local Thermal Equilibrium, a unique  $n_e$  may be calculated from each temperature after the manner of BLADES [36]. Reversing the theoretical formulas to obtain the corresponding  $T_{n_e, \text{LTE}}$  from a measured  $n_e$  is difficult but a third-order polynomial was found to fit the two parameters well over

the range of  $T = 6500$  to  $10,000$  K and  $n_e = 1 \times 10^{13}$  to  $1 \times 10^{16}$  cm.<sup>-3</sup> This relationship is:

$$T_{n_e, \text{LTE}} = 5475 + 1026(X) - 64.32(X^2) + 58.12(X^3) \quad (5)$$

where  $X = \log_{10}(n_e) - 13$  in order to reduce round-off errors. This formula was useful in determining theoretical equilibrium temperatures based on experimental electron density measurements.

### 3. RESULTS and DISCUSSION

#### 3.1. Physical Parameters of the Discharge

3.1.1. Excitation Temperatures. Figures 3 and 4 present iron excitation temperatures determined at the several power levels as a function of observation height in the plasma, using the critically evaluated transition probabilities. When the different transition probability data sets and power levels are taken into account, a real comparison can be made between this study and those of other researchers who have investigated the vertical spatial profile of the excitation temperature at 27 MHz. FURUTA and HORLICK [37] made observations at a single fairly high power level of 1800 W, which would be expected to give high temperatures, but used CORLISS and BOZMAN's [11] transition probabilities, which then bring the reported temperatures down. KAWAGUCHI et al. [38] made observations at three different power levels and used transition probabilities from REIF et al. [23], which as expected give slightly higher temperatures than obtained in this study. Both of these groups observed a similar dip in excitation

temperature at low observation heights, and this dip is seen to move lower in the plasma as power is increased in the present investigation as well.

While the 27 MHz plasma exhibits a strong power level dependence of the excitation temperatures, the very high frequency plasma does not. This is in accordance with their visual appearance when a 1000 ppm solution of yttrium is aspirated. With a nebulizer gas flow of 0.7 L/min, the blue ionic emission region in the so-called "Normal Analytical Zone" [39,40] begins approximately 15 mm above the load coil at the lower frequency, with increasing intensity observed with increasing power. The VHF discharge at 900 W does not develop this emission region, but remains a red color throughout in the standard size torch. At higher powers, a small blue patch develops about 15 mm above the load coil, but remains very faint even at 1500 W.

That higher frequencies yield lower excitation temperatures in the ICP has been previously demonstrated [4,5], so a lower temperature is not unexpected for the 148 MHz plasma. The effects of different power levels and specific observation heights were not addressed in their paper, so the linear relationship between temperature and frequency shown by CAPELLE et al. [4] may only be fortuitous. If that relationship is extended to 148 MHz, negative temperatures would have been expected, clearly an unrealistic situation. Since calcium emission lines were used for the excitation temperatures in the other frequency study [5], only the similarity in trend can be noted there.



3.1.2. Electron Densities. The calculated electron densities as a function of power and observation height in the two plasmas are shown in Figs. 5 and 6. Many researchers have reported electron densities only at a single observation height and power level. For example, the value of  $5 \times 10^{15} \text{ cm}^{-3}$  at 1500 W and 15 mm observation height determined by UCHIDA et al. [41] at 27 MHz is slightly higher than our value of  $3.5 \times 10^{15} \text{ cm}^{-3}$  under similar conditions, while  $1.6 \times 10^{15} \text{ cm}^{-3}$  from REZAAIYAN and HIEFTJE [35] is slightly lower. ALDER et al. [42] showed electron densities over the range 10 mm - 25 mm observation height for one power of 1200 W which are only slightly higher than the observed curve for 1250 W at 27 MHz. Axial values extracted from the spatial data of CAUGLIN and BLADES [43] are also similar. Although these spatial data indicate higher electron densities outside of the central channel at low observation heights, the lack of Abel inversion techniques should not affect the validity of the lateral measurements, especially for heights greater than 8 mm, because the electron densities in the present study were derived from  $H\beta$  emission from injected water, which is mainly confined to the anlayte channel.

Figures 5 and 6 show a fairly smooth drop in electron density with observation height and a direct dependence on power level for both ICPs. The 148 MHz discharge exhibits about half an order of magnitude lower electron density overall, and in contrast to the excitation temperature, a direct power level dependence is observed. The lower electron density is expected from other workers' results at higher frequencies [10,44] but again if the linear trend shown by CAPELLE et al. [4] is continued the predicted

electron density at 148 MHz would be seven orders of magnitude lower than is actually observed.

3.1.3. Ion to Atom Line Ratios. It has been stated that a relative idea of electron density can be easily obtained from the ratio of ionic to atomic emission from a suitable element [4]. Magnesium is often used because of the proximity of the Mg(I) line at 285.21 nm and two Mg(II) lines at 279.55 and 280.27 nm. When LTE is assumed,  $T_{\text{exc}} = T_{\text{ion}} = T_{\text{LTE}}$  and the Saha and Boltzmann equations can be combined to yield the following relationship between electron density and ion/atom emission ratios:

$$\frac{I^+}{I^0} = \frac{2\pi (2 m_e k)^{3/2}}{n_e h^3} \frac{g^+ A^+ / \lambda^+}{g^0 A^0 / \lambda^0} T_{\text{LTE}}^{3/2} \exp \left( \frac{-E_{\text{ion}} - E_{\text{exc}} + E_{\text{exc}}}{k T_{\text{LTE}}} \right) \quad (6)$$

where  $n_e$  = electron density (in  $\text{m}^{-3}$ ),

$m_e$  = electron mass ( $9.11 \times 10^{-31}$  kg),

$k$  = Boltzmann's constant ( $1.381 \times 10^{-23}$  J/K or  $0.6947 \text{ cm}^{-1}/\text{K}$ ),

$h$  = Planck's constant ( $6.626 \times 10^{-34}$  J-s),

$I^0, I^+$  = emission intensity of neutral and ionized species,

$g^0, g^+$  = statistical weight of the emitting level in the atom and ion,

$A^0, A^+$  = transition probability,

$\lambda^0, \lambda^+$  = wavelength of emission.

$E_{\text{ion}}$  = ionization energy,

$E_{\text{exc}}^{\text{r}}, E_{\text{exc}}^{\text{s}}$  = excitation energy of the emitting level

in the atom and ion,

$T_{\text{LTE}}$  = temperature.

The emission intensity ratio is dependent not only on electron density, but also on the temperature. Since the excitation temperature has been shown to vary dramatically with power and observation height, a simple measurement of the  $\text{Mg(II)}/\text{Mg(I)}$  ratio will not strictly follow the electron density, as can be seen in Figs. 7 and 8, which show the observed Mg ratios for the two frequencies. Electron density values calculated from observed ion/atom intensity ratios and excitation temperatures are often orders of magnitude lower than  $n_e$  values obtained from Stark broadening measurements [34]. Indeed, experimental ion/atom emission intensity ratios have been proposed as a measure of the deviation from LTE [43].

The values reported for the ratio of  $\text{Mg(II)}/\text{Mg(I)}$  emission at single observation heights and power levels by KALNICKY *et al.* [34] and CAPELLE *et al.* [4] are about twice the observed value of this ratio under similar conditions, but the vertical spatial behavior shown by FURUTA and HORLICK [37] agrees well with these observations. The vertical spatial profile deduced from data presented by CAUGHLIN and BLADES [43] is also similar in shape to that obtained in the present study. The differences may be due to the lack of Abel inversion of the ion and atom intensities here.

A dramatic effect of observation height is seen at 27 MHz, roughly corresponding to the different zones of the plasma observed with yttrium

introduced: lower in the plasma principally atomic emission is observed, while the ionic emission is maximized in the Normal Analytical Zone and then falls off with increasing height. In the 148 MHz plasma, the blue ionic emission is much less intense, and the  $Mg(II)/Mg(I)$  ratios are lower as well. In addition, the influence of power level is less pronounced. These effects are consistent with the changes in excitation temperature and electron density seen above.

### 3.2. Analytical Performance

3.2.1. Signal to Background Ratios. Generally, the signal to background ratio was found to be strongly dependent on observation height. Typical behavior is shown in Fig. 9 for copper(I) at 324.75 nm. Low in the plasma, the S/B ratio was low, and increased to a maximum about 30-33 mm above the load coil. Applying the method of WINGE *et al.* [45], one might conclude that this observation height would provide the best detection limit. The best actual detection limits however are not strictly a function of the S/B ratio [3,46]. At this height, the background was indeed very low, but so was the net signal, and with a limited amount of gain available in the electrometer, the lowest detection limits were not obtained. The maximum net signal for most elements was found to be 17-20 mm above the load coil for both frequencies. In this spatial region, the actual detection limits were reasonably close to those approximated from the S/B ratios. Results for the observation heights at which the detection limits were obtained are summarized and compared in Table 3. The signal to background ratio decreases with increasing frequency in all cases except  $Ca(I)$  at

422.67 nm. Because the background intensity decreases similarly for all the transitions, the S/B ratio changes primarily in response to the decreasing net signal intensity, with ion lines more sensitive to the frequency change than the atom lines.

3.2.2. Detection Limits. A compromise observation height of 19.5 mm above the load coil based on the signal to background ratio measurements was used for all elements except calcium. The maximum net signal for calcium was found to be 13 mm above the load coil for both frequencies and, interestingly, for both the atom and ion emission lines.

The detection limit was based on the concentration of analyte that gave an average signal equal to twice the peak-to-peak noise of the baseline actually evaluated at that concentration. A time constant of 0.1 sec was used. The results at 27 MHz are generally 5-10 times higher than those tabulated by WINGE et al. [45], but are not unreasonable considering the differences in instrumentation.

Since identical procedures and instrumentation were used at both frequencies, a valid comparison can be made between these two plasmas. Results are summarized in Table 4. In all cases except the Fe(I) and Ca(I) lines, the detection limit at 148 MHz is higher than that at 27 MHz. The trend in general follows the trend in signal to background ratios: the ion emission lines decrease more than the atom lines, so the atom line detection limits are closer to the 27 MHz values than those determined from the ion lines. This is in contrast to the results found previously [4], in which S/B ratios and detection limits improve with frequency up to 56 MHz.

Apparently, analytical performance improves at twice the conventional frequency, but does not continue the trend with a six-fold increase.

3.2.3. Calibration Curves. Calibration curves are linear and extend over four or more orders of magnitude for both frequencies, as can be seen from the representative curves shown in Fig. 10. Calcium was the only element found to fall off significantly at 1000 ppm at 27 MHz, but was found to be linear to 1000 ppm at 148 MHz. All other curves were found to be strictly linear at both frequencies, with similar dynamic ranges.

3.2.4. Interferences. The vaporization interference of phosphate on a 3  $\mu\text{g/mL}$  solution of calcium was investigated at both frequencies, and was not found to be of significant magnitude up to molar ratios of 700:1  $\text{PO}_4^{3-}:\text{Ca}$ . At a ratio of 1300:1, a 5 percent depression of the atomic emission occurs for both frequencies, as shown in Fig. 11. The ionic emission is essentially unaffected at 27 MHz, while at 148 MHz a slightly greater depression is seen. The six-fold increase in frequency does not reduce the ICP's insensitivity to this interference.

3.2.5. Organics. In order to determine the relative ease of sample introduction, many common organic solvents were aspirated into the two plasmas, including acetone, benzene, hexane, methanol, and xylene. "Organic iron" solutions were prepared from ferrocene dissolved in benzene and xylene. In order to operate the 27 MHz ICP with the organic solvents, drastic retuning (several turns of each variable capacitor in the matching

network) and a minimum power level of 1500 W was necessary. Less drastic retuning was also necessary for different classes of compounds. Even under these conditions, it was difficult to keep the plasma lit. At 148 MHz, only the more volatile species required a slight retuning (1/8 turn of one of the capacitors) and power levels as low as 650 W operated satisfactorily.

The difference in the appearance of the two plasmas was striking when benzene was aspirated. At 27 MHz, the usual "green tongue" was seen in a generally green plasma, with a slight amount of yellow emission from incomplete combustion accompanied by some soot formation. At 148 MHz, the yellow emission was more intense, giving an extremely bright plasma and larger quantities of soot. All other solvents in both plasmas were simply green. Because of this high background emission, the most sensitive scales of the electrometer could not be used at the higher frequency with benzene as the solvent, and xylene was used instead.

At 27 MHz and 1500 W, the Fe(I) line at 371.99 nm gave 16 times more signal than the ion line at 259.94 nm, in contrast to the behavior with aqueous solutions. The atom line at 148 MHz and 1200 W provided the same size signal as at 27 MHz, with approximately equal noise on the same electrometer setting. Sensitivity is therefore about equal for the two frequencies with organic solvents, but the high frequency plasma's improved tolerance for organic solvents at lower powers is a distinct advantage.

### 3.3 Approach to LTE

It has recently been suggested that the electron density, being a single-valued parameter amenable to determination without already assuming

Local Thermal Equilibrium, is most appropriate to characterize a discharge in LTE, rather than an excitation temperature, which may be dependent on the element involved and the excitation energies of the levels used [42,43,48]. This provides a basis for comparing the deviation from LTE in an actual plasma. The observed  $n_e$  data translate to the  $T_{n_e, \text{LTE}}$  curves shown in Figs. 12 and 13. Transition probabilities taken from SMITH and LISZT [49] and other spectroscopic data used in the calculation of theoretical intensity ratios by Eqn. (6) are listed in Table 5. The parameter  $b_r$  introduced by CAUGHLIN and BLADES is then simply obtained:

$$b_r = \frac{(I^+/I^0)_{\text{expt}}}{(I^+/I^0)_{\text{LTE}}} \quad (7)$$

Values of  $b_r$  calculated from these data are shown in Figs. 14 and 15. Since electron densities were found to fall smoothly with height, the  $b_r$  values follow the spatial behavior of the  $\text{Mg(II)}/\text{Mg(I)}$  intensity ratios. In all cases,  $b_r$  is less than one, reflecting the use of  $T_{n_e, \text{LTE}}$  rather than  $T_{\text{exc}}$  in the LTE calculation. The values at 27 MHz are slightly less than those shown by CAUGHLIN and BLADES, largely due to the difference in Mg ratios. It is not clear at this time what range of variation may be expected from laboratory to laboratory due to differences in instrumentation or techniques. Comparing the two frequencies in a single laboratory, it can be seen that the 148 MHz ICP deviates much more strongly from LTE than the 27 MHz ICP. As observation height is increased, the two plasmas approach a similar state of non-LTE.



### 3.4. Discussion

The detection limits in the 148 MHz plasma are higher than those at 27 MHz primarily because the signal has fallen off faster than the background. The increase in detection limits roughly corresponds to the decrease in signal to background ratio. At all wavelengths observed, the background was 5-12 times lower at 148 MHz. This is primarily due to the 3-fold drop in electron density from 27 MHz and 1000 W to 148 MHz and 1200W, since the background continuum emission is proportional to the square of the electron density [44].

The decrease in electron density does not scale directly with frequency, which is understandable when the skin depth is considered. The skin depth decreases by a factor of 2.4 over this frequency range if the same power levels are maintained, and this directly affects the relationship between the energy deposition region and the analyte channel. Comparing equivalent power levels at each frequency, i.e. 1200 W and 1500 W, the electron density is 5 times lower at 148 MHz, which is twice the change in skin depth. It is difficult to apply this hypothesis to studies by other researchers at intermediate frequencies because of the different experimental conditions employed. GUNTER et al. [5] did not directly determine the electron densities, and CAPELLE et al. [4] only show measured electron densities for 5, 27 and 40 MHz. Since the 5 MHz ICP was operated at five times the power of the other two, direct comparison cannot be made. From 27 to 40 MHz, the skin depth is expected to decrease by a factor of 1.2, while their observed  $n_e$  drops by 1.7. Differences in applied power or other experimental parameters not reported in their paper may be the reason

this result does not compare directly with the present study. Scaling with skin depth rather than directly with frequency better explains the observed magnitude of the decrease in electron density with frequency.

The reason behind the decrease in emission intensity is not so clear. The excitation temperature drops by a factor of 1.5 over this frequency range. Neither the excitation temperature nor the decrease in analyte emission seem to be simply correlated with the change in skin depth. The relative loss of net signal intensity might be roughly related to the excitation energy of the emitting levels of the atom lines, but this correlation does not hold for the ion lines, even when the ionization potential is taken into account. FURUTA and HORLICK [37] have proposed that neutral atom excitation is a result of electron collisions, while collisions with excited argon species are responsible for the generation and excitation of ionic species. The lower electron densities would lead to the lower emission intensities under this scenario, and the different behavior of the ion lines could be rationalized.

Values of  $b_p$  less than one are said to be indicative of an ionizing non-equilibrium plasma undergoing rapid heating, characterized by a relative over-population of ground state levels compared to LTE [44]. The shift farther from LTE is evidenced by the shift of the Mg ion/atom intensity ratio towards atom emission with increased frequency. The same behavior is seen for the other elements for which both atomic and ionic emission data were obtained. At 27 MHz the Fe(II) line is approximately six times the intensity of the Fe(I) line, while it is only about half as intense at 148 MHz. Similarly, at 27 MHz the calcium ion line is 100 times more

intense than the atom line, but at 148 MHz they are of approximately equal intensity. Two effects have combined here to cause this: the drop in electron density serves to shift ionization equilibria away from the ion, and the greater relative over-population of the ground state causes the atom lines to decrease less relative to the ion lines as frequency increases.

#### 4. CONCLUSION

These investigations of an analytical ICP at a frequency nearly three times higher than any previously reported demonstrate the effects of the reduced skin depth at higher generator frequencies. This produces a less energetic environment characterized by lower excitation temperatures and electron densities, resulting in both lower background and analyte emission from the VHF plasma. The background intensity is proportional to the square of the electron density, which scales with the skin depth rather than directly with the frequency. The analyte emission is a more complex function which falls off faster than the background over this extended frequency range. The observed shift away from ionic emission is indicative of a shift farther from LTE as skin depth is reduced. The ICP's immunity to interelement interferences is not lost at 148 MHz and ease of sample introduction, especially of organic species, is improved.

#### ACKNOWLEDGMENT

This research was partially supported by the Office of Naval Research.

## REFERENCES

- [1] T. B. REED, J. Appl. Phys. 32, 921 (1961).
- [2] T. B. REED, J. Appl. Phys. 32, 2534 (1961).
- [3] R. H. SCOTT, V. A. FASSEL, R. N. KNISELEY and D. E. NIXON, Anal. Chem. 46, 75 (1974).
- [4] B. CAPELLE, J. M. MERMET and J. ROBIN, Appl. Spectrosc. 36, 102 (1982).
- [5] W. H. GUNTER, K. VISSER and P. B. ZEEMAN, Spectrochim. Acta 38B, 949 (1983).
- [6] D. L. WINDSOR, D. R. HEINE and M. B. DENTON, Appl. Spectrosc. 33, 56 (1979).
- [7] D. R. HEINE, J. S. BABIS and M. B. DENTON, Appl. Spectrosc. 34, 595 (1980).
- [8] S. B. TILDEN and M. B. DENTON, J. Autom. Chem. 1, 128 (1979).
- [9] D. J. KALNICKY, R. N. KNISELEY and V. A. FASSEL, Spectrochim. Acta 30B, 511 (1975).
- [10] J. JAROSZ, J. M. MERMET and J. ROBIN, Spectrochim. Acta 33B, 55 (1978).
- [11] C. H. CORLISS and W. R. BOZMAN, Experimental transition probabilities for spectral lines of seventy elements, National Bureau of Standards Monograph 53, United States Department of Commerce, Washington, D.C. (1962).
- [12] C. H. CORLISS and J. L. TECH, Oscillator strengths and transition probabilities for 3288 lines of Fe I, National Bureau of Standards Monograph 108, United States Department of Commerce, Washington, D.C. (1968).
- [13] C. H. CORLISS and J. L. TECH, J. Res. Natn. Bur. Stand. 80A, 787 (1976).
- [14] J. M. BRIDGES and R. L. KORNBLITH, Astrophys. J. 192, 793 (1974).
- [15] D. E. BLACKWELL and B. S. COLLINS, Mon. Not. R. Astr. Soc. 157, 255 (1972).
- [16] D. E. BLACKWELL, P. A. IBBETSON and A. D. PETFORD, ibid. 177, 195 (1975).

- [17] D. E. BLACKWELL, P. A. IBBETSON and A. D. PETFORD, ibid. 177, 219 (1975).
- [18] D. E. BLACKWELL, P. A. IBBETSON, A. D. PETFORD and M. J. SHALLIS, ibid. 186, 633 (1979).
- [19] D. E. BLACKWELL, A. D. PETFORD and M. J. SHALLIS, ibid. 186, 657 (1979).
- [20] D. E. BLACKWELL and M. J. SHALLIS, ibid. 186, 669 (1979).
- [21] D. E. BLACKWELL, A. D. PETFORD, M. J. SHALLIS and G. J. SIMMONS, ibid. 191, 445 (1980).
- [22] J. R. FUHR, G. A. MARTIN, W. L. WIESE and S. M. YOUNGER, J. Phys. Chem. Ref. Data 10, 305 (1981).
- [23] I. REIF, V. A. FASSEL, R. N. KNISELEY and D. J. KALNICKY, Spectrochim. Acta 33B, 807 (1978).
- [24] L. M. FAIRES, B. A. PALMER, R. ENGLEMAN, JR. and T. M. NIEMCZYK, Spectrochim. Acta 39B, 819 (1984).
- [25] J. D. ALGEO and M. B. DENTON, Appl. Spectrosc. 35, 25 (1981).
- [26] W. L. WIESE and J. R. FUHR, J. Phys. Chem. Ref. Data 4, 263 (1975).
- [27] J. R. ROBERTS, T. ANDERSEN and G. SORENSEN, Astrophys. J. 181, 567 (1973).
- [28] J. R. ROBERTS, P. A. VOIGHT and A. CZERNECHOWSKI, Astrophys. J. 197, 791 (1975).
- [29] B. WARNER, Mem. R. Astr. Soc. 70, 165 (1967).
- [30] W. L. WIESE, Plasma Diagnostic Techniques, (edited by R. H. Huddleston and S. L. Leonard), Chapter 6. Academic Press, New York, (1965).
- [31] H. R. GRIEM, Plasma Spectroscopy. McGraw-Hill, New York, (1964).
- [32] H. R. GRIEM, Spectral Line Broadening by Plasmas. Academic Press, New York, (1974).
- [33] C. R. VIDAL, J. COOPER and E. W. SMITH, Astrophys. J. Suppl. Series No. 214, 25, 37-136 (1973).
- [34] D. J. KALNICKY, V. A. FASSEL and R. N. KNISELEY, Appl. Spectrosc. 31, 137 (1977).

- [35] R. REZAAIYAAN and G. M. HIEFTJE Anal. Chem. 57, 412 (1985).
- [36] M. W. BLADES, Spectrochim. Acta 37B, 869 (1982).
- [37] N. FURUTA and G. HORLICK, Spectrochim. Acta 37B, 53 (1982).
- [38] H. KAWAGUCHI, T. ITO and A. MIZUIKE, Spectrochim. Acta 36B, 615 (1981).
- [39] S. R. KOIRTYOHANN, J. S. JONES and D. A. YATES, Anal. Chem. 52, 1965 (1980).
- [40] S. R. KOIRTYOHANN, J. S. JONES, C. P. JESTER and D. A. YATES, Spectrochim. Acta 36B, 49 (1981).
- [41] H. UCHIDA, K. TANABE, Y. NOJIRI, H. HARAGUCHI and K. FUWA, Spectrochim. Acta 36B, 711 (1981).
- [42] J. F. ALDER, R. M. BOMBELKA and G. F. KIRKBRIGHT, Spectrochim. Acta 35B, 163 (1980).
- [43] B. L. CAUGHLIN and M. W. BLADES, Spectrochim. Acta 39B, 1583 (1984).
- [44] G. R. KORNBLUM and L. DeGALAN, Spectrochim. Acta 32B, 71 (1977).
- [45] K. R. WINGE, V. J. PETERSON and V. A. FASSEL, Appl. Spectrosc. 33, 206 (1979).
- [46] R. J. LUKASIEWICZ and F. G. DEWALT, I. C. P. Inf. Newslett. 9, 730 (1984).
- [47] N. FURUTA, C. W. McLEOD, H. HARAGUCHI and K. FUWA, Appl. Spectrosc. 34, 211 (1980).
- [48] I. J. M. M. RAAIJMAKERS, P. W. J. M. BOUMANS, B. VAN DER SIJDE, and D. C. SCHRAM, Spectrochim. Acta 38B, 697 (1983).
- [49] W. H. SMITH and H. S. LISZT, J. Opt. Soc. Am. 61, 938 (1971).

Table 1. Iron(I) Line Data for Excitation Temperature Calculations

$\lambda$ (nm)	$E_{\text{exc}}$ ( $\text{cm}^{-1}$ )	$\log(gf)^a$	$\log(gf)^b$	$\log(gf)^c$	$\log(gf)^d$
371.994	26875	-.430	-.43	-.17	-.28
372.762	34547	-.631	-.52	-.40	-.24
373.487	33695	.317	.31	.57	.62
373.713	27167	-.574	-.57	-.31	-.49
374.949	34040	.161	.17	.41	.43
381.584	38175	.30	.25	.42	.56

<sup>a</sup>Ref. [22]

<sup>b</sup>Ref. [14]

<sup>c</sup>Ref. [23]

<sup>d</sup>Ref. [11]

Table 2. Titanium(II) Line Data for  
Excitation Temperature Calculations

$\lambda$ (nm)	$E_{exc}$ (cm <sup>-1</sup> )	$\log(gf)^a$
321.706	31301	-.45
322.284	31114	-.40
322.913	30959	-.47
323.452	31301	.26
324.860	40798	.58
325.291	30959	-.49

<sup>a</sup>Ref. [29]



Table 3. Comparison of Signal to Background Ratios

Element	$\lambda$ (nm)	$E_{exc}$ ( $cm^{-1}$ )	$E_{ion}$ ( $cm^{-1}$ )	<u>Ratio 27 MHz/148 MHz</u>		
				<u>Bkgd</u>	<u>S-B</u>	<u>S/B</u>
Ca I	422.67	23652		11	5	0.5
Ca II	393.37	25414	49285	12	794	48
Cu I	324.75	30782		7	46	-
Fe I	371.99	26875		10	31	3
Fe II	259.94	38459	63424	7	619	42
Mg I	285.21	35051		5	105	16
Mg II	279.55	35671	61649	5	333	43
Ni I	341.48	29481		5	32	4
V II	309.31	35843	49035	9	131	11

Table 4. Detection Limits ( $\mu\text{g/mL}$ )

Element	$\lambda$ (nm)	Reference <sup>a</sup>	27 MHz	148 MHz	Ratio 148/27
Ca I	422.67	0.01	0.1	0.1	1
Ca II	393.37	0.0002	0.001	0.1	100
Cu I	324.75	0.005	0.05	0.5	10
Fe I	371.89	0.07 <sup>b</sup>	0.5	0.5	1
Fe II	259.94	0.006	0.05	2.	40
Mg I	285.21	0.002	0.02	0.5	25
Mg II	279.55	0.0002	0.005	0.3	60
Ni I	341.48	0.05	1.	3.	3
V II	309.31	0.005	0.03	0.5	17

<sup>a</sup>Ref. [45], except Fe I.

<sup>b</sup>Ref. [47]

Table 5. Magnesium Line Data

Species	$\lambda$ (nm)	$E_{\text{exc}}$ ( $\text{cm}^{-1}$ )	$g$	$A$ ( $\text{s}^{-1}$ ) <sup>a</sup>	$E_{\text{ion}}$ ( $\text{cm}^{-1}$ )
Mg I	280.27	35671	2	$2.7 \times 10^8$	61649
Mg II	285.21	35051	3	$5.26 \times 10^8$	

<sup>a</sup>Ref. [49]

## FIGURE CAPTIONS





Fig. 1. Iron(I) excitation temperatures determined using several different transition probability data sets at 27 MHz and 1000 W. Transition probabilities from:  FUHR et al. [22],  BRIDGES and KORNBLITH [14],  REIF et al. [23],  CORLISS and BOZMAN [11].





Fig. 2. Titanium(II) and iron(I) excitation temperatures determined at 27 MHz.  titanium at 1000 W,  iron at 1000 W,  titanium at 1250 W,  iron at 1250 W.

Fig. 3. Iron(I) excitation temperatures at 27 MHz.  800 W,  1000 W,  1250 W,  1500 W.

Fig. 4. Iron(I) excitation temperatures at 148 MHz.  900 W,  1200 W,  1500 W.





Fig. 5. Electron densities determined from Stark broadening at 27 MHz.  800 W,  1000 W,  1250 W,  1500 W.




Fig. 6. Electron densities determined from Stark broadening at 148 MHz.  900 W,  1200 W,  1500 W.

Fig. 7. Magnesium ion (279.55 nm) to atom (285.21 nm) emission intensity ratios determined at 27 MHz. ■ 800 W, ○ 1000 W, ▲ 1250 W, □ 1500 W.

Fig. 8. Magnesium ion (279.55 nm) to atom (285.21 nm) emission intensity ratios determined at 148 MHz. ○ 900 W, ▲ 1200 W, □ 1500 W.

Fig. 9. Copper(I) signal to background ratios and relative signal intensities determined at 324.75 nm under compromise operating conditions. ○ 27 MHz and 1000 W, □ 148 MHz and 1200 W.

Fig. 10. Analytical calibration curves for □ Fe(II) (259.94 nm) and ○ Cu(I) (324.75 nm) at 27 MHz and 1000 W, ■ Fe(I) (371.99 nm) and ▲ Cu(I) (324.75 nm) at 148 MHz and 1200 W.

Fig. 11. Effect of phosphate on calcium ion and atom emission intensity from a 3 µg/mL solution. ○ 27 MHz and 1000 W, □ 148 MHz and 1200 W.

Fig. 12. LTE temperatures determined from electron densities at 27 MHz.

■ 800 W, ○ 1000 W, ▲ 1250 W, □ 1500 W.

Fig. 13. LTE temperatures determined from electron densities at 148 MHz.

○ 900 W, ▲ 1200 W, □ 1500 W.

Fig. 14. Values of  $b_r = (I^+/I^0)_{\text{expt}} / (I^+/I^0)_{\text{LTE}}$  calculated for 27 MHz.

■ 800 W, ○ 1000 W, ▲ 1250 W, □ 1500 W.

Fig. 15. Values of  $b_r = (I^+/I^0)_{\text{expt}} / (I^+/I^0)_{\text{LTE}}$  calculated for 148 MHz.

○ 900 W, ▲ 1200 W, □ 1500 W.

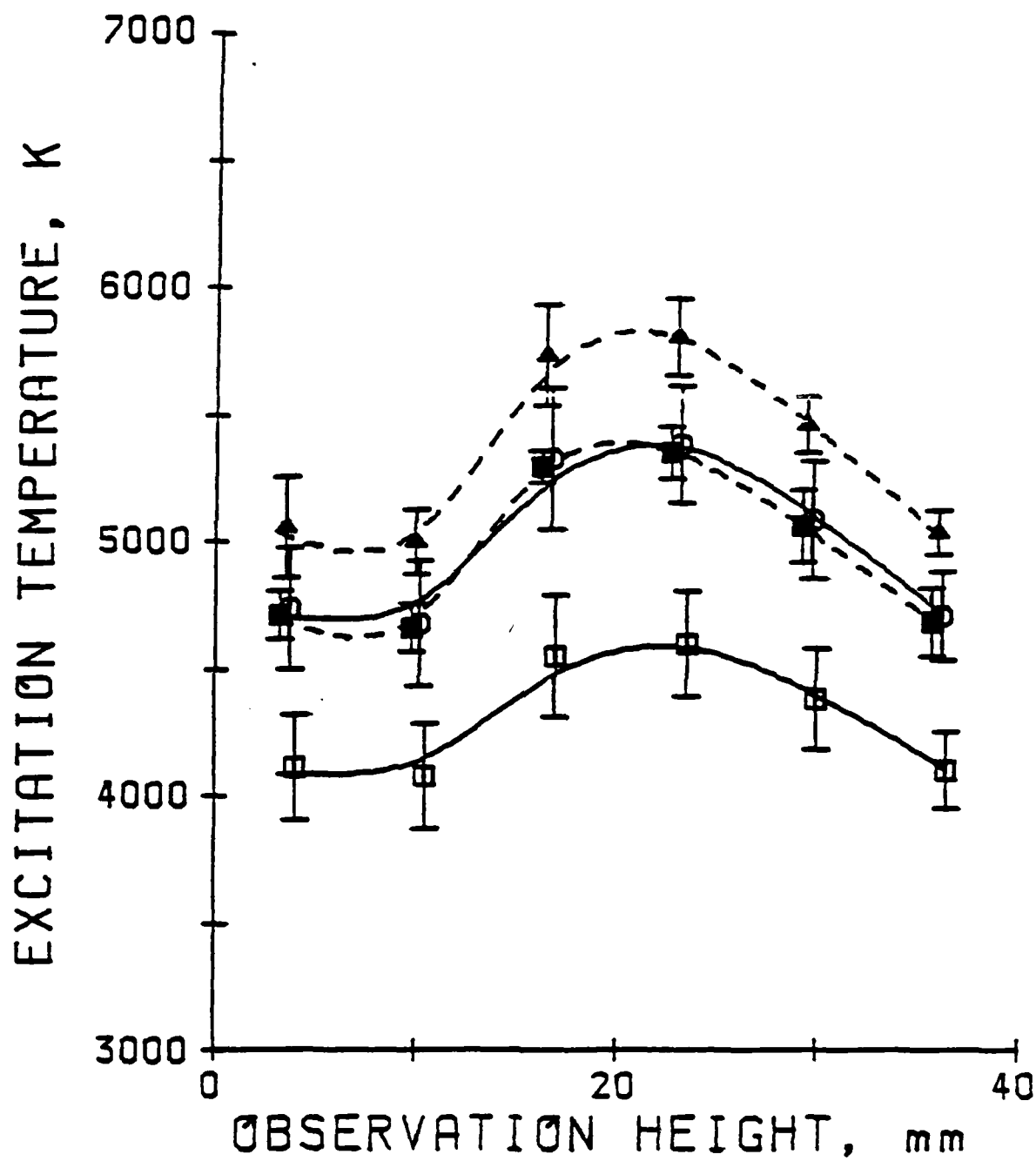


Figure 1

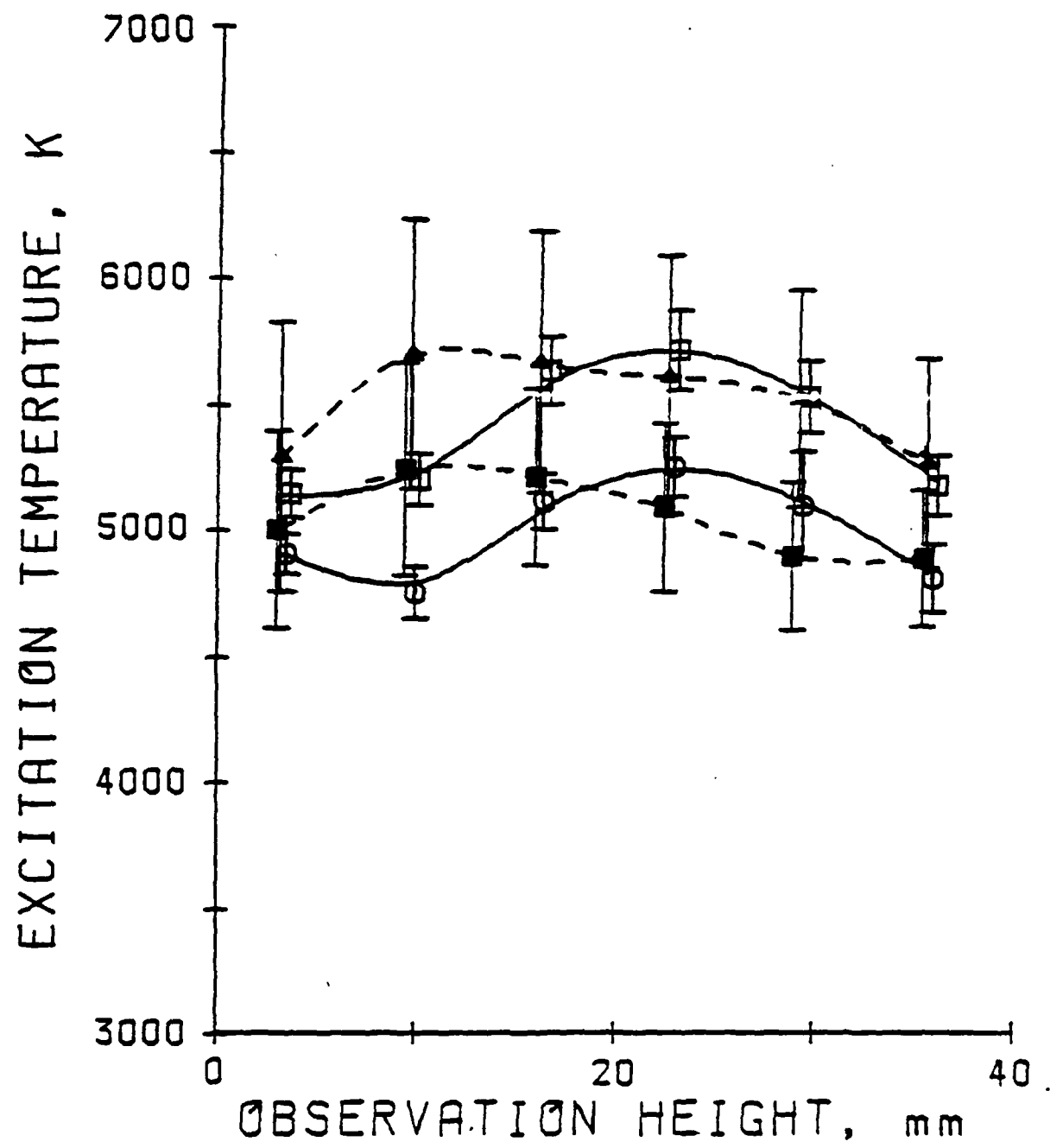


Figure 2



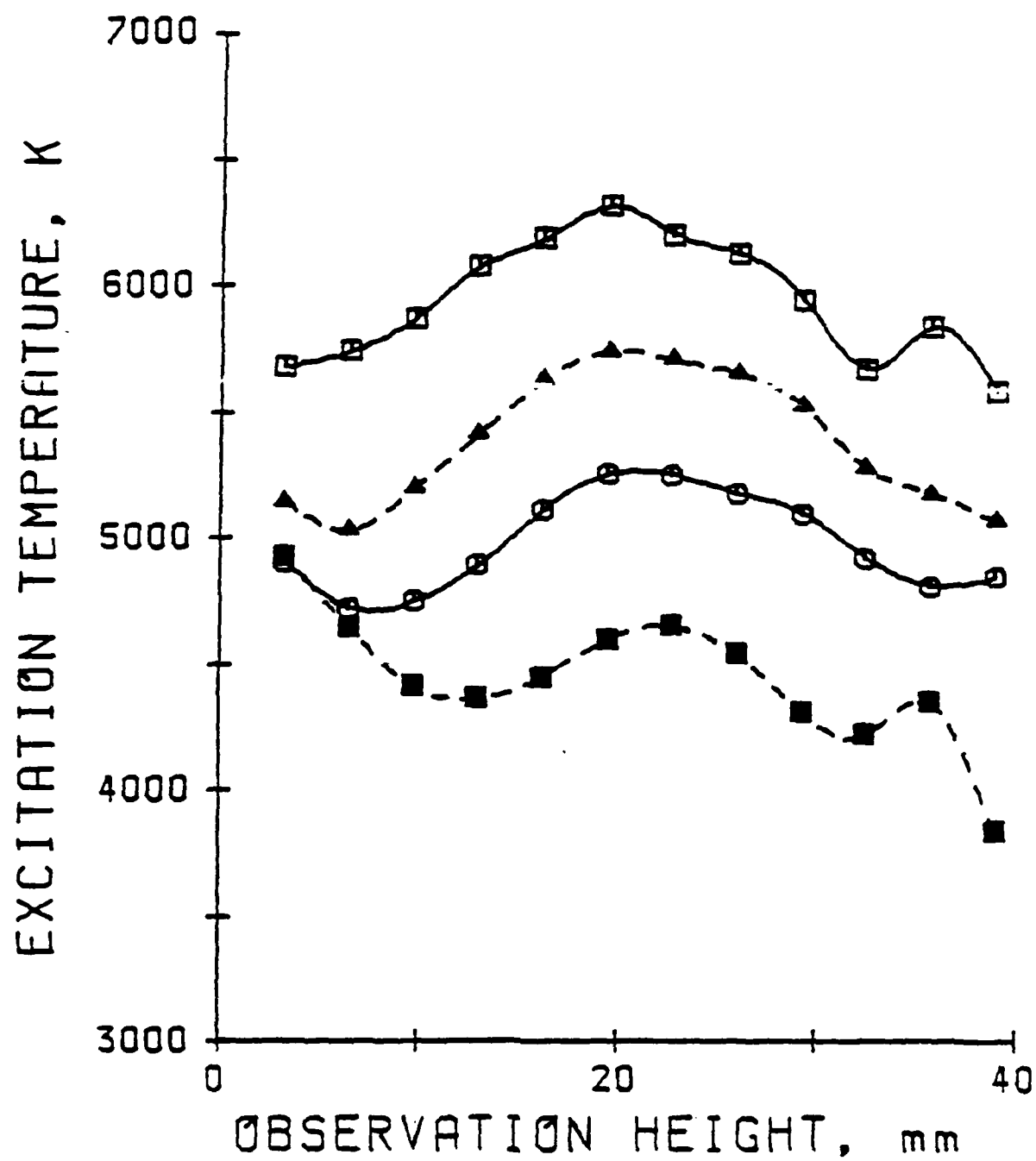


Figure 3

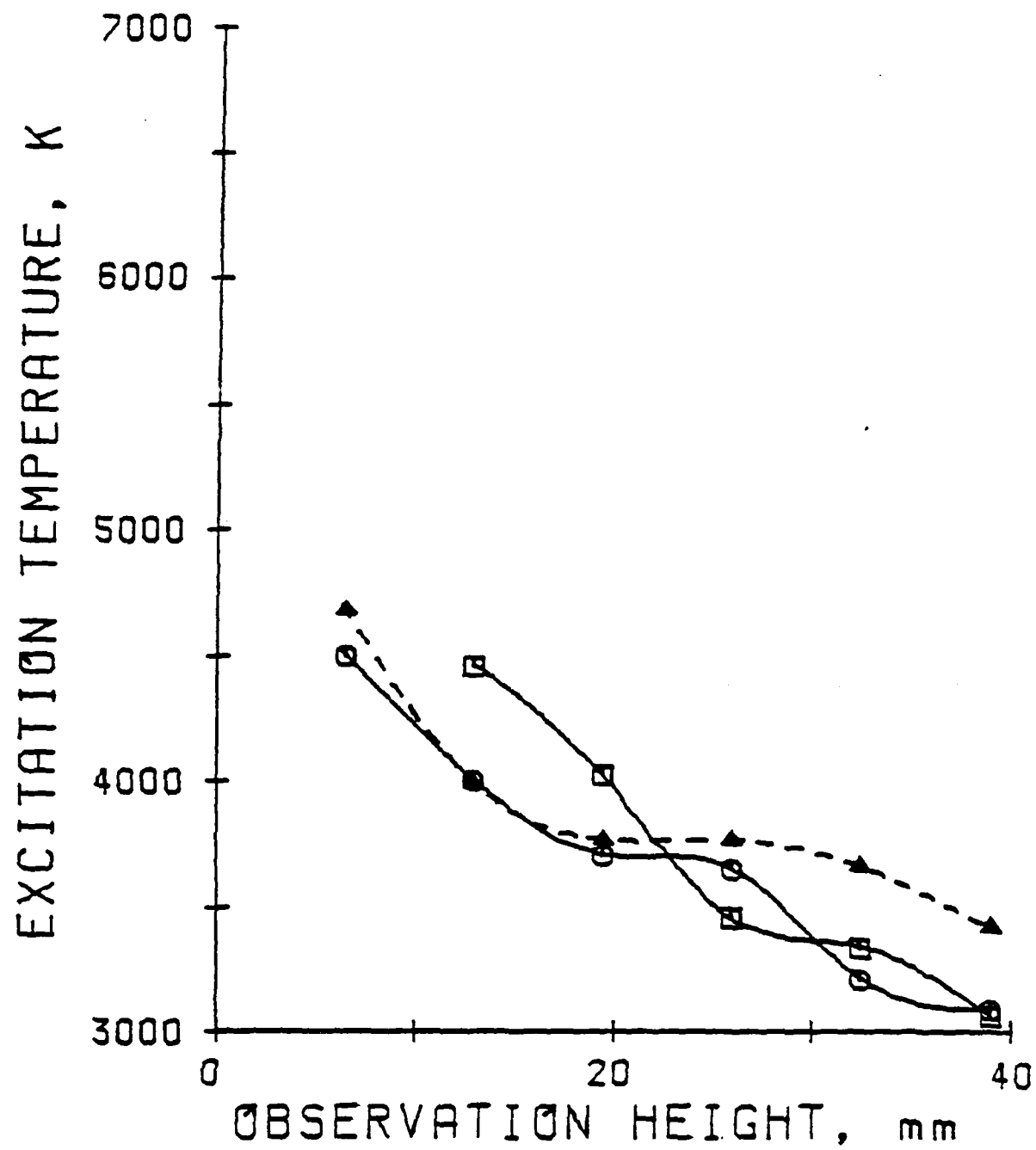


Figure 4

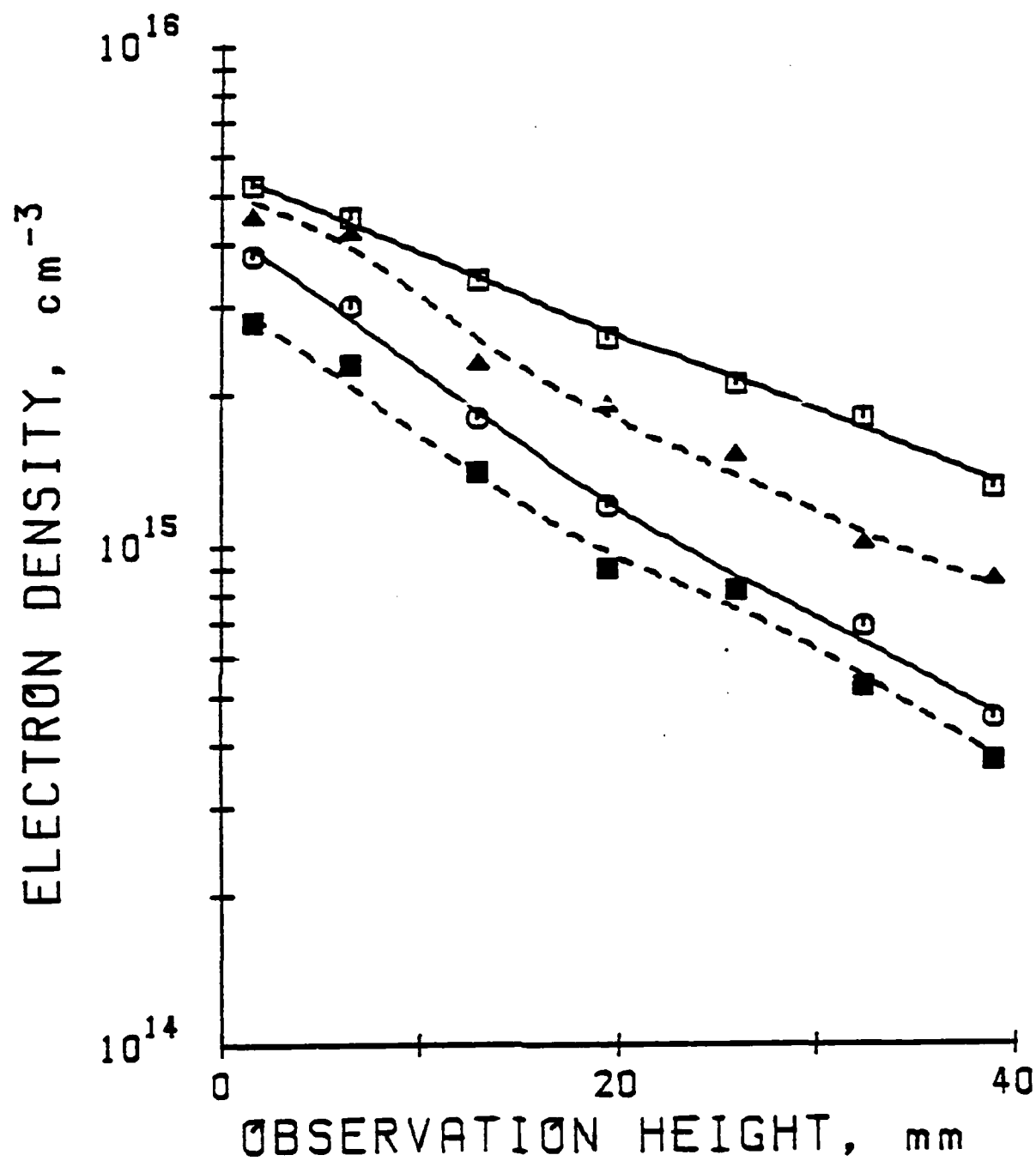


Figure 5

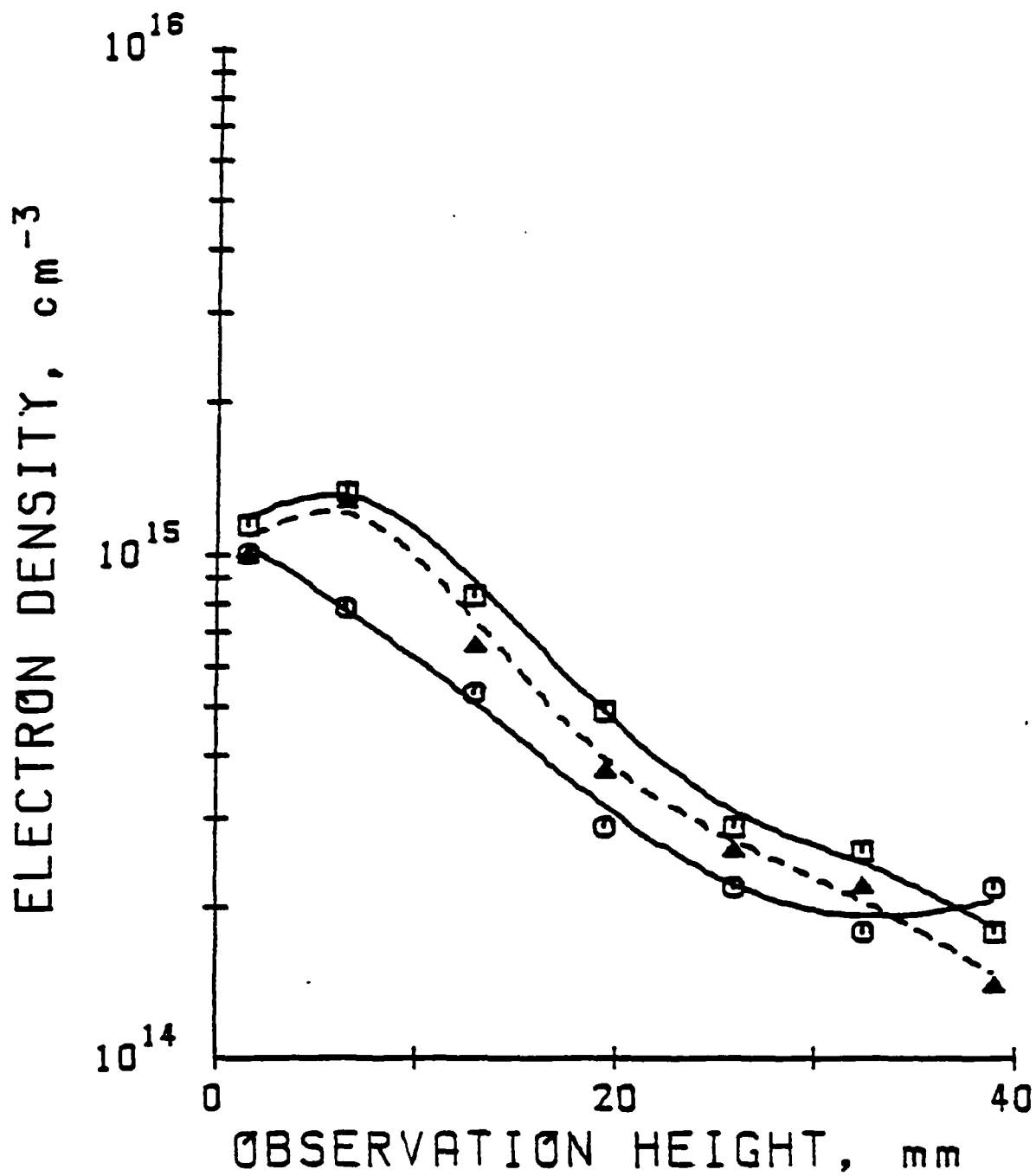


Figure 6

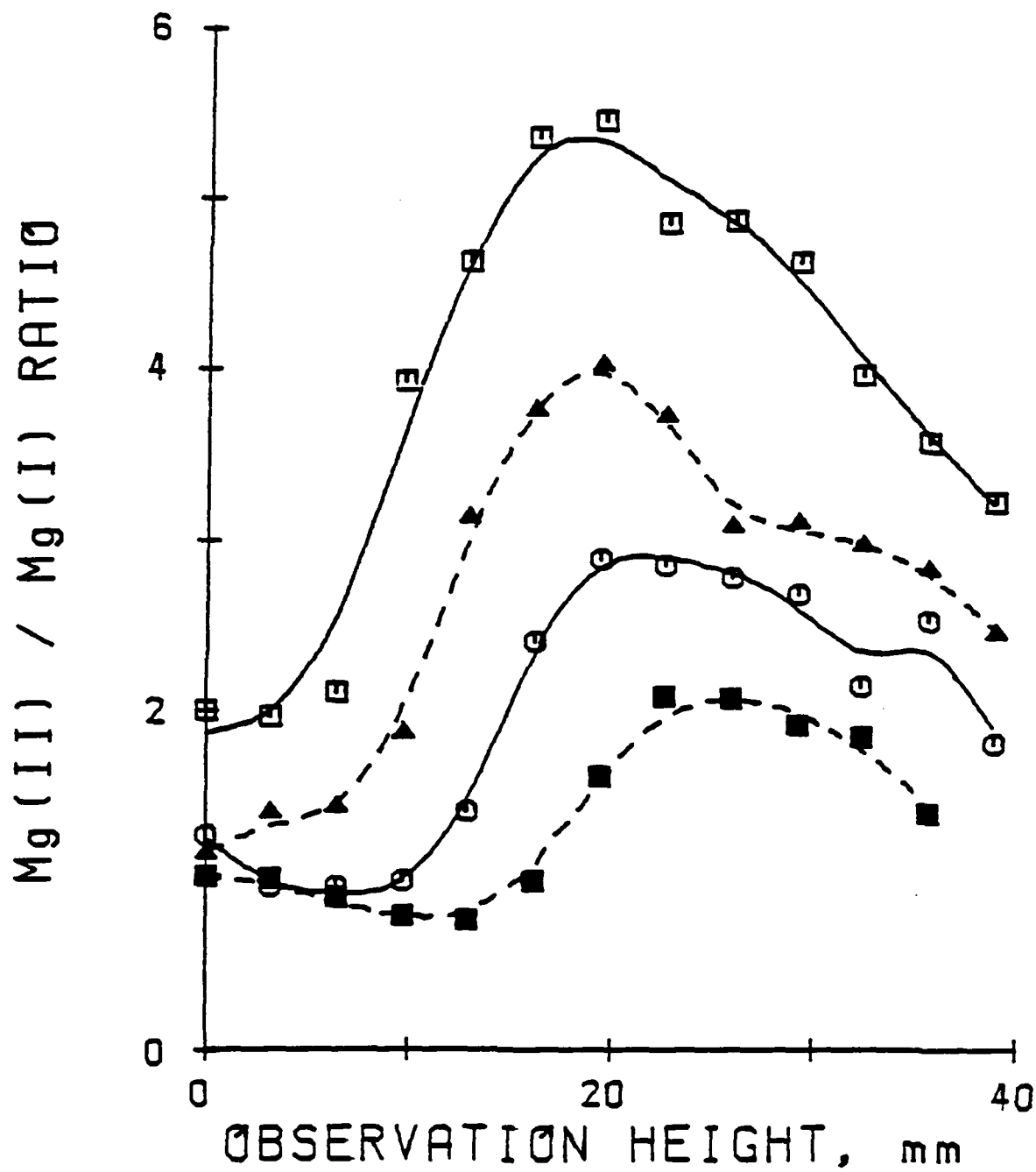


Figure 7

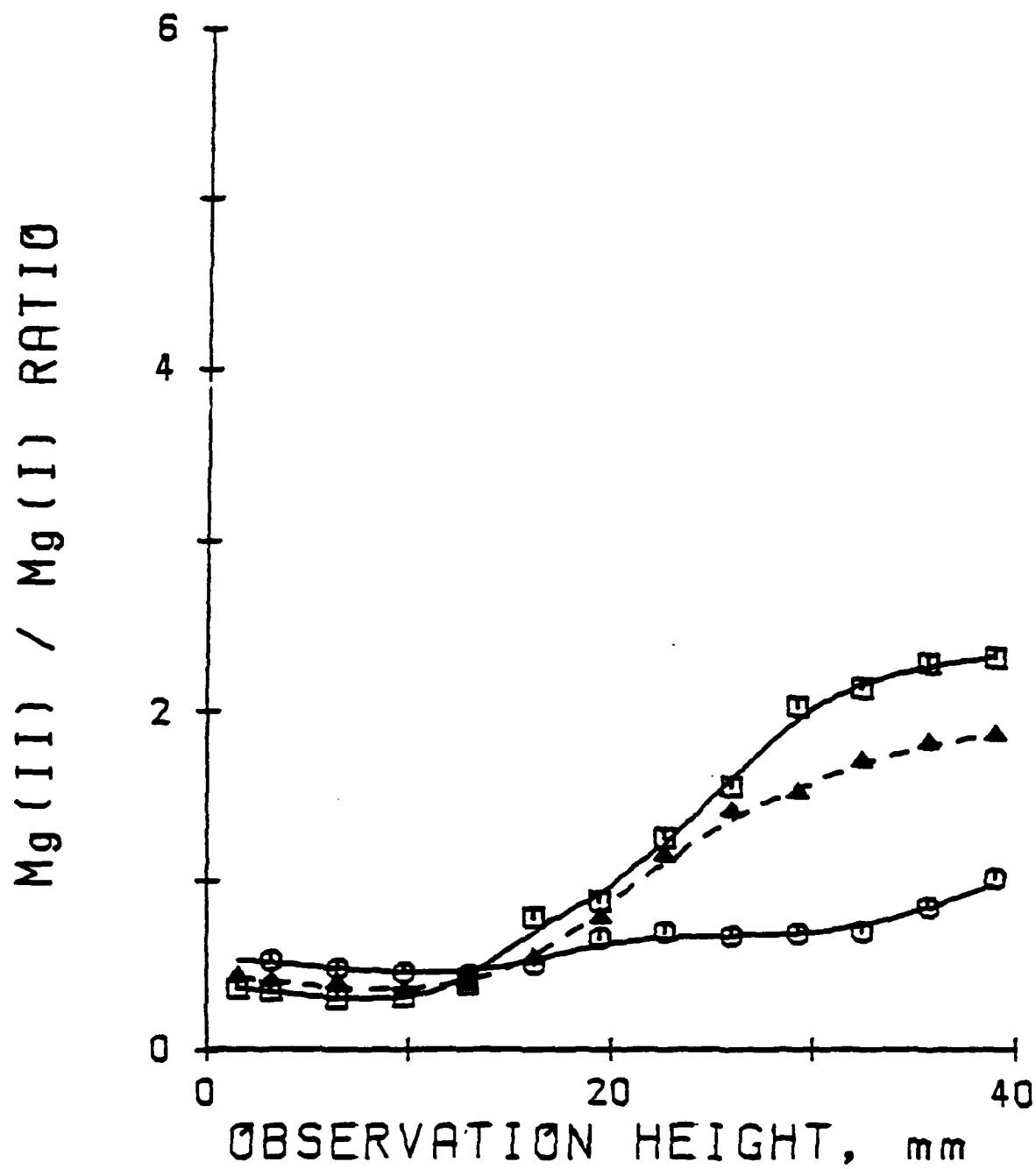


Figure 8

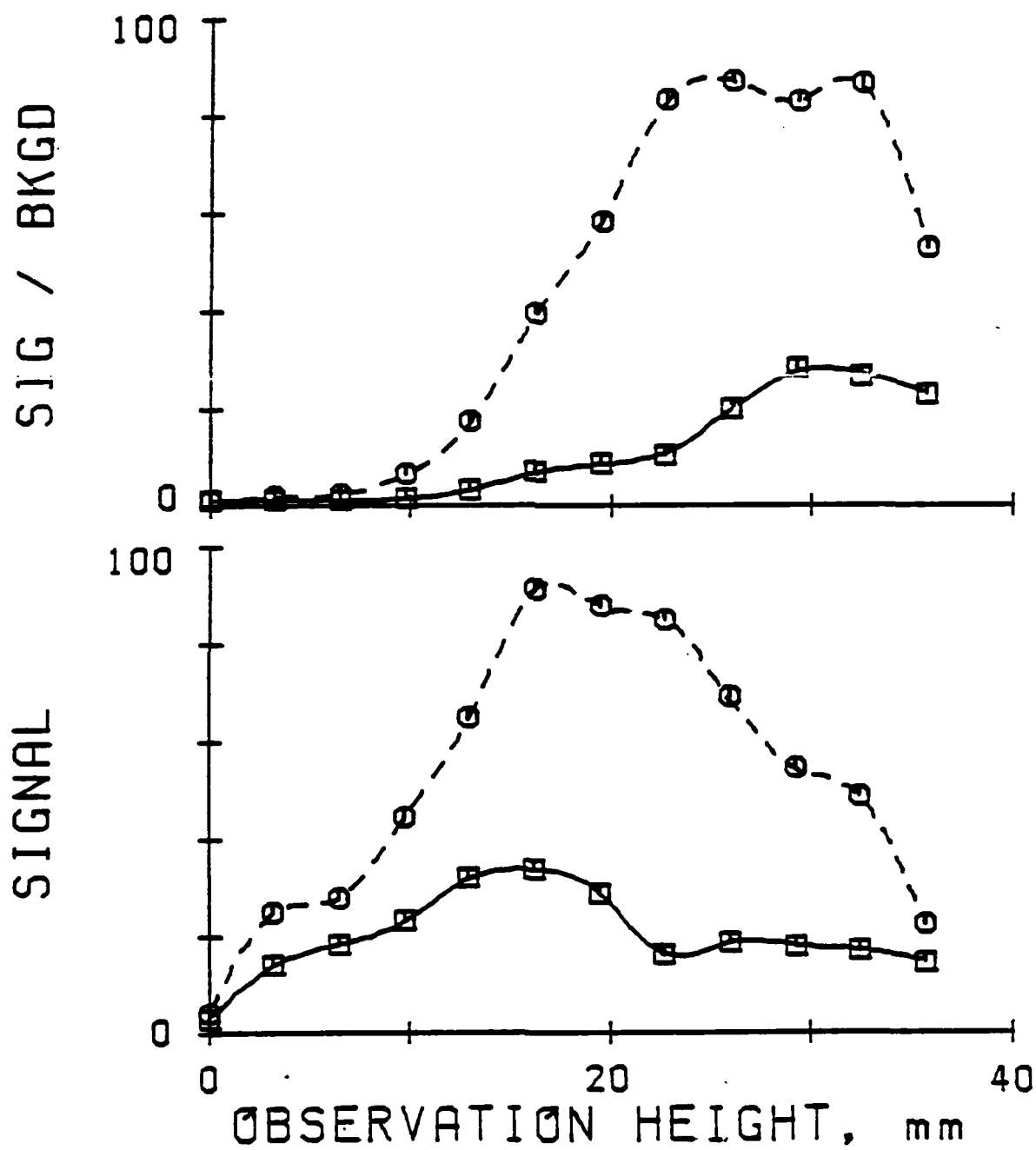


Figure 9

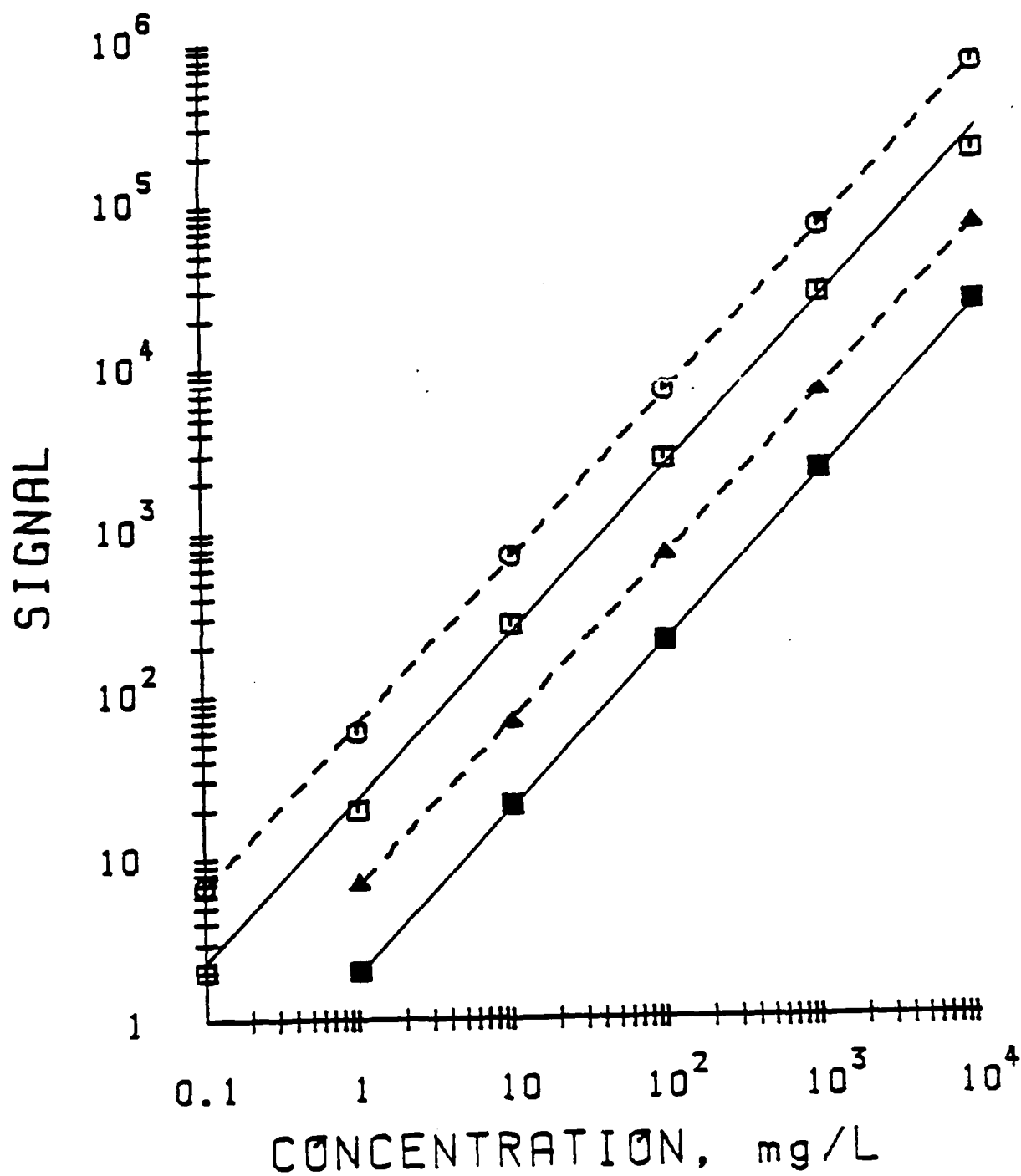


Figure 10



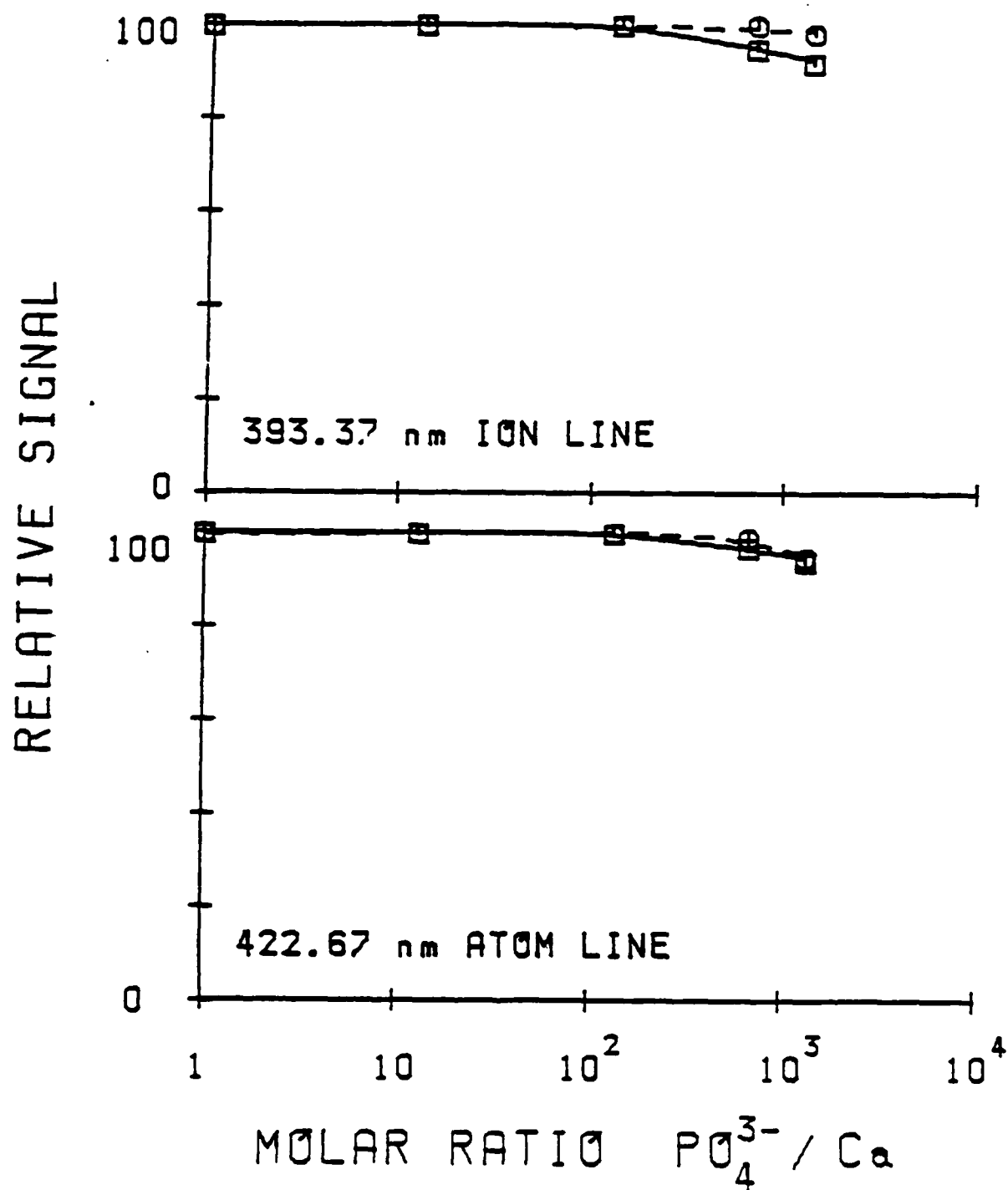


Figure 11

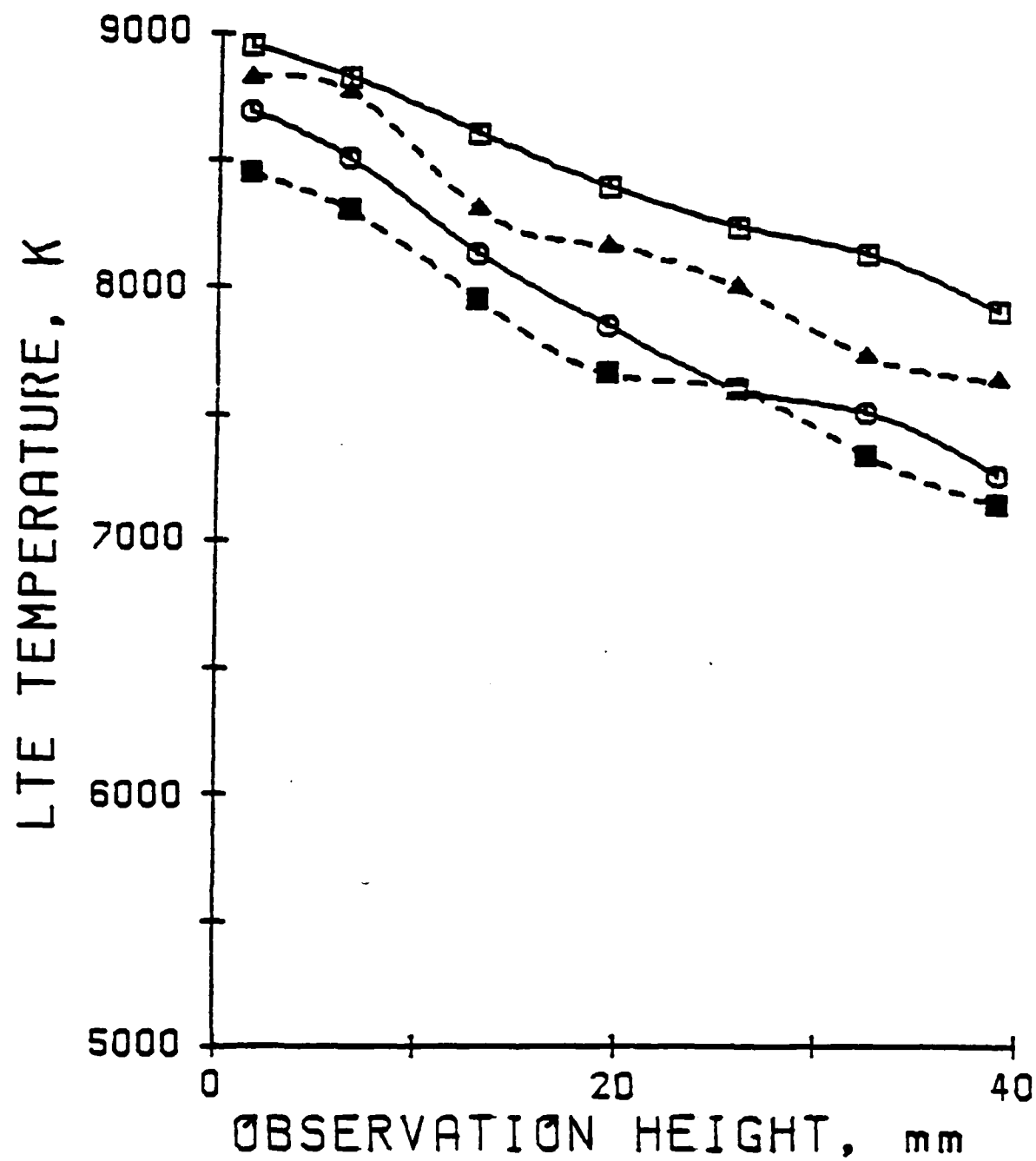


Figure 12

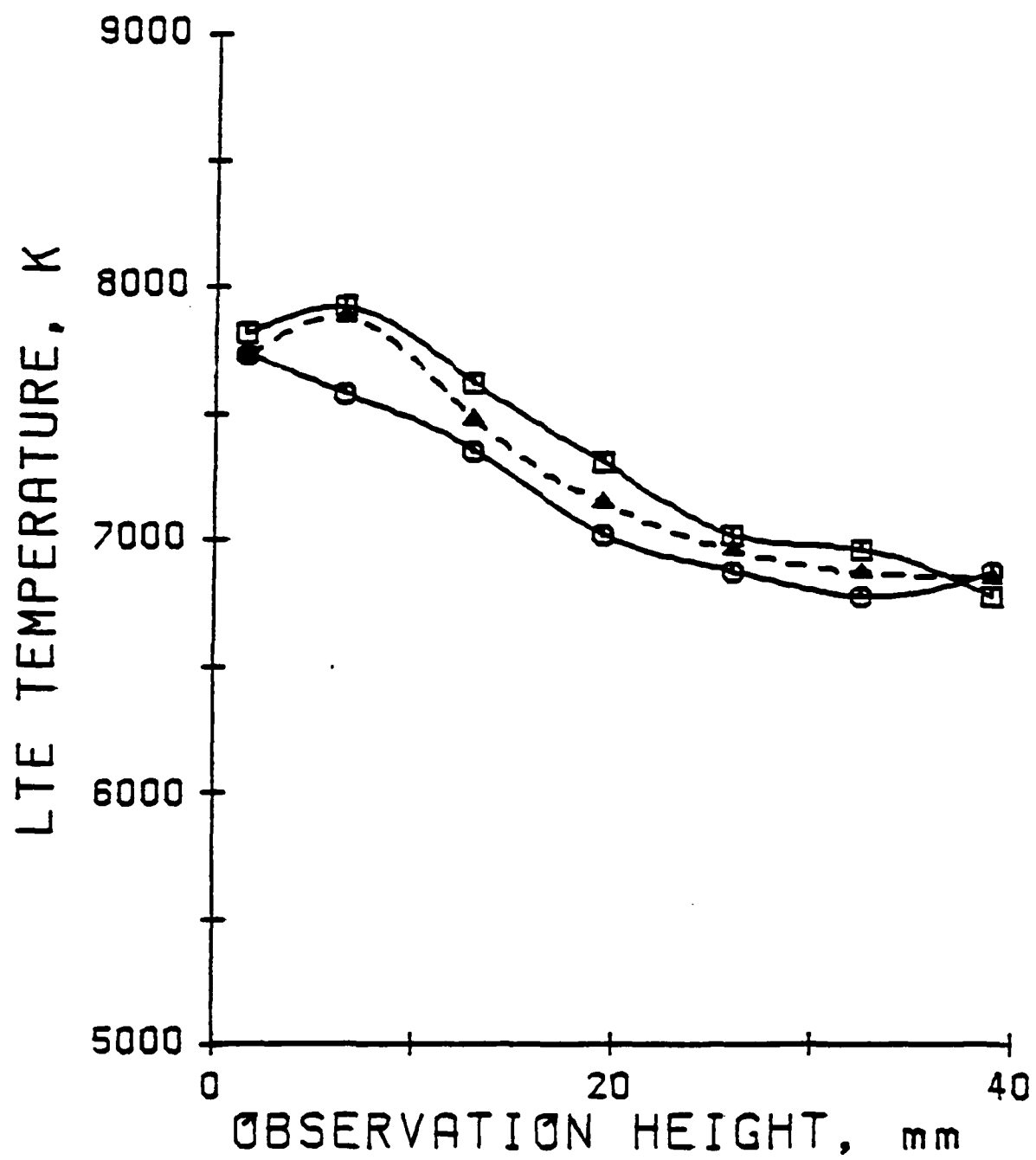


Figure 13

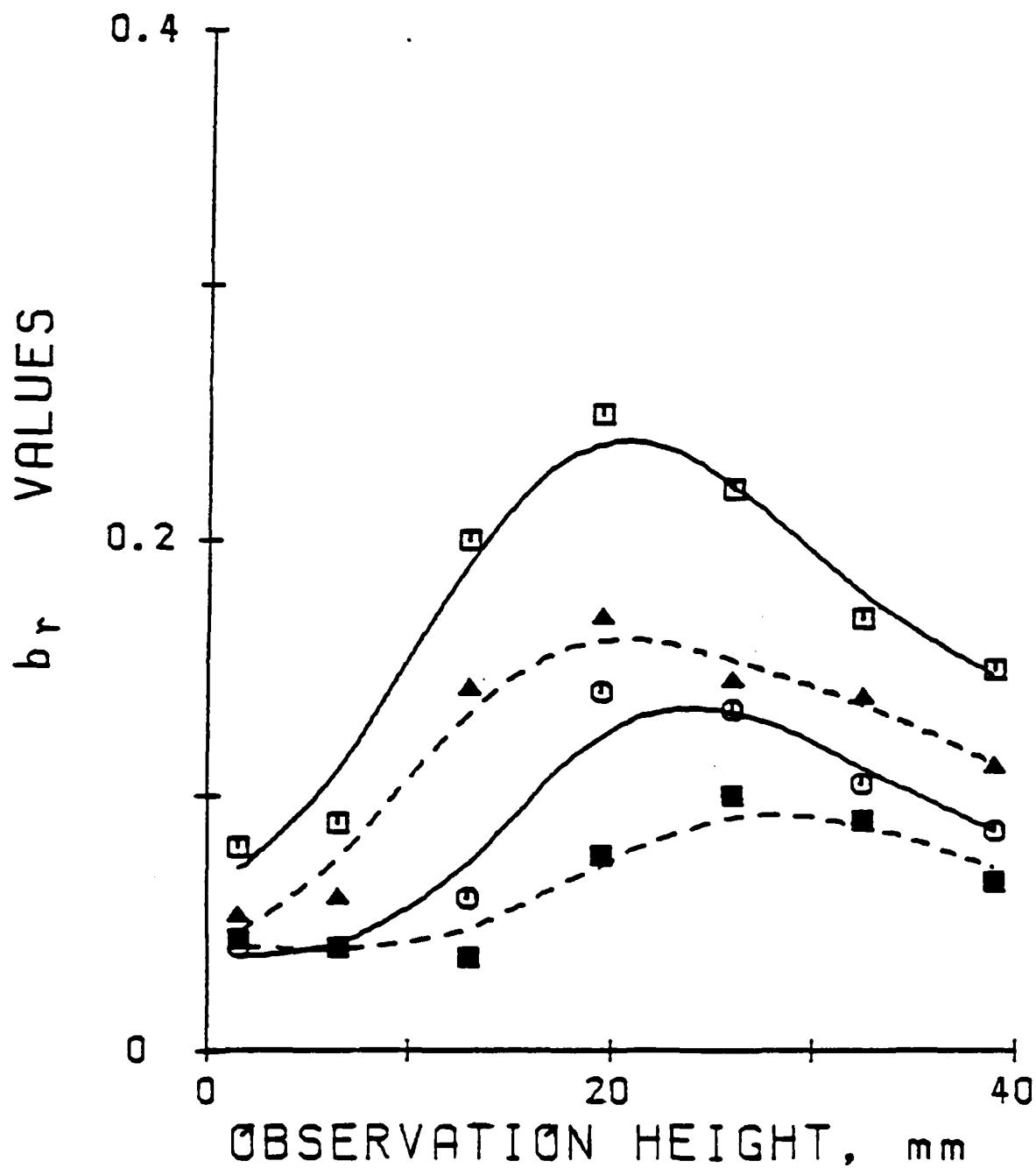


Figure 14

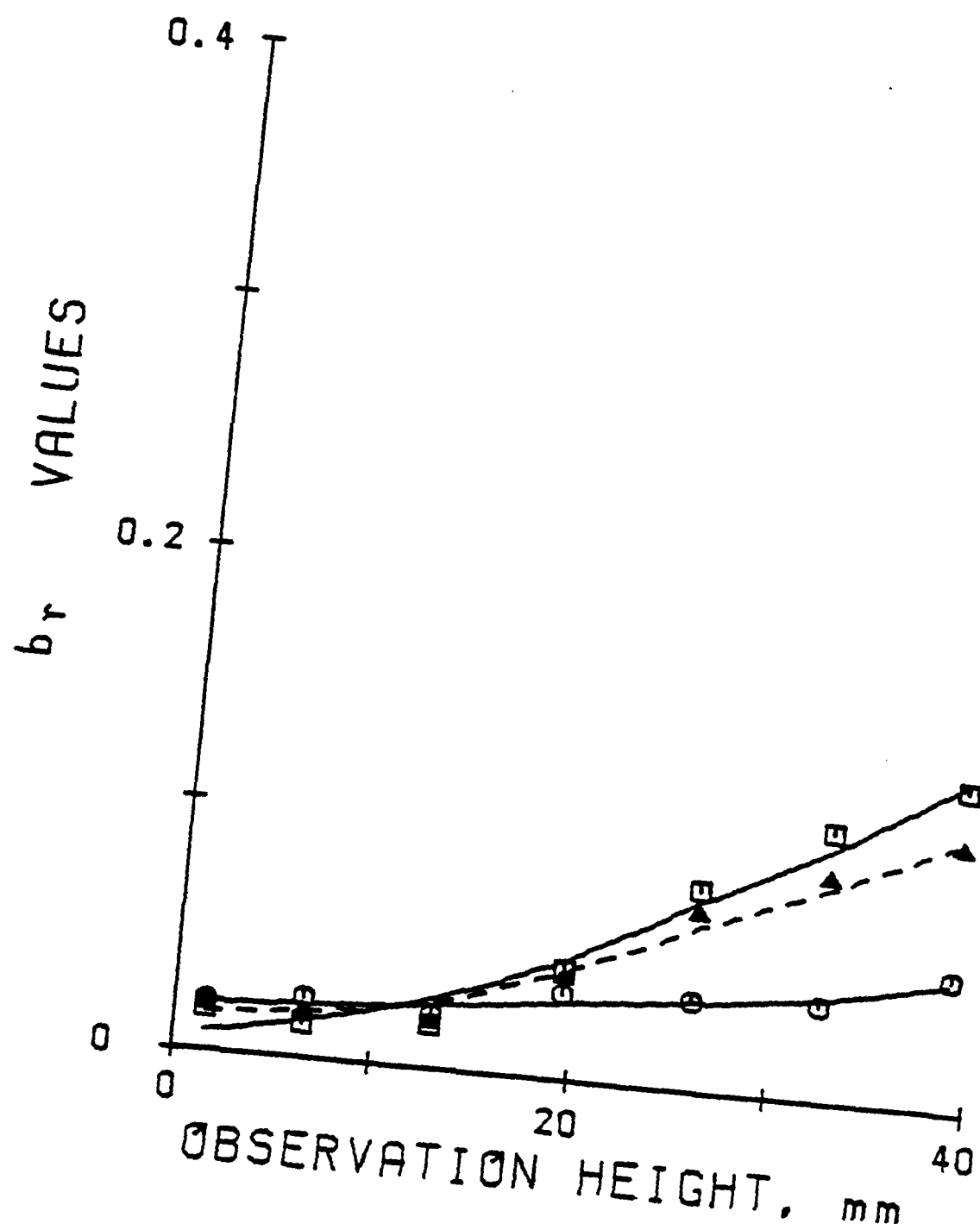


Figure 15

**END**

**FILMED**

---

*2-86*

**DTIC**